

Can a heavy $U(1)_{B-L}$ Z' boson explain the muon $(g-2)_\mu$ anomaly?

António P. Morais^{a,b,1,*} Roman Pasechnik^{b,c,d,1,†} and J. Pedro Rodrigues^{a1,‡}

^{1a}*Departamento de Física da Universidade de Aveiro and CIDMA Campus de Santiago, 3810-183 Aveiro, Portugal*

^b*Department of Astronomy and Theoretical Physics, Lund University, SE 223-62 Lund, Sweden*

^c*Nuclear Physics Institute ASCR, 25068 Řež, Czech Republic*

^d*Departamento de Física, CFM, Universidade Federal de Santa Catarina, C.P. 476, CEP 88.040-900, Florianópolis, SC, Brazil*

The minimal $U(1)_{B-L}$ extension of the Standard Model (B-L-SM) offers an explanation for both neutrino mass generation via a seesaw mechanism and the observed anomaly in the muon $(g-2)_\mu$. The emergence of a second Higgs particle as well as a new Z' gauge boson, both linked to the breaking of a local $U(1)_{B-L}$ symmetry, makes the B-L-SM rather constrained by direct searches at the Large Hadron Collider (LHC) experiments. We investigate how well the observed $(g-2)_\mu$ anomaly can be reproduced in the B-L-SM while simultaneously confronting the new physics predictions with the LHC and electroweak precision data. Taking into account the current bounds from direct LHC searches, we demonstrate that the $(g-2)_\mu$ anomaly can still be explained by means of Z' boson if its mass lies in a range of 5 to 20 TeV.

arXiv:1912.11882v1 [hep-ph] 26 Dec 2019

* aapmorais@ua.pt

† Roman.Pasechnik@thep.lu.se

‡ joapedrorodrigues@ua.pt

I. INTRODUCTION

It is unquestionable that the Standard Model (SM) is a successful framework accurately describing the phenomenology of Particle Physics up to the largest energy scales probed by collider measurements so far. In fact, contemporary direct searches for new physics or indirect probes via e.g. flavour anomalies, have been showing an increasingly puzzling consistency with SM predictions. However, it is not less true that the SM also possesses its weaknesses and several open questions are yet to be understood. One of such weaknesses is a missing explanation of tiny neutrino masses confirmed by flavour-oscillation experiments. The minimal way of addressing this problem is by adding heavy Majorana neutrinos in order to realise a seesaw mechanism [1–3]. However, the mere introduction of an arbitrary number of heavy neutrino generations can raise new questions, in particular, how such a new scale is generated from a more fundamental theory.

Among the simplest ultraviolet (UV) complete theories that dynamically addresses this question is the minimal gauge- $U(1)_{B-L}$ extension of the SM [4–6], traditionally dubbed as the B-L-SM. As its name suggests, the B-L-SM promotes an accidental conservation of the difference between baryon (B) and lepton (L) numbers in the SM to a fundamental local Abelian symmetry group. Furthermore, such a $U(1)_{B-L}$ symmetry can be embedded into larger groups such as e.g. $SO(10)$ [7–11] or E_6 [12–14], making the B-L-SM model well motivated by Grand Unified Theories (GUTs). The presence of three generations of right-handed neutrinos also ensures a framework free of anomalies with their mass scale developed once the $U(1)_{B-L}$ is broken by the VEV of a complex SM-singlet scalar field, simultaneously giving mass to the corresponding Z' boson.

The cosmological implications of the B-L-SM are also relevant. First, the presence of an extended neutrino sector implies the existence of a sterile state that can play a role of keV- to TeV-scale Dark Matter candidate [15]. Particularly, it can be stabilized by imposing a \mathbb{Z}_2 parity as it was done e.g. in Refs. [16, 17]. The $U(1)_{B-L}$ model with sterile neutrino Dark Matter can also explain the observed baryon asymmetry via the leptogenesis mechanism (see Refs. [18–20], for details). As was mentioned earlier, the B-L-SM features an extended scalar sector with a complex SM-singlet state χ which, besides enriching the Higgs sector with a new potentially visible state, can cure the well-known metastability of the electroweak (EW) vacuum in the SM [21–23]. Indeed, it was shown in Ref. [24] that an additional physical scalar with a mass beyond a few hundred GeV can stabilize the Higgs vacuum all the way up to the Plank scale. In the framework of B-L-SM, a complete study of the scalar sector was performed in Ref. [25] where the vacuum stability conditions valid at any Renormalization Group (RG) scale were derived. Last, but not least, the presence of the complex SM-singlet χ interacting with a Higgs doublet typically enhances the strength of EW phase transition potentially converting it into a strong first-order one [26].

Another open question that finds no solution in the SM is the discrepancy between the measured anomalous magnetic moment of the muon, $a_\mu^{\text{exp}} \equiv \frac{1}{2}(g-2)_\mu^{\text{exp}}$, and its theoretical prediction, $a_\mu^{\text{SM}} \equiv \frac{1}{2}(g-2)_\mu^{\text{SM}}$, which reads [27]

$$\Delta a_\mu = a_\mu^{\text{exp}} - a_\mu^{\text{SM}} = 268(63)(43) \times 10^{-11} \quad (1)$$

with numbers in brackets denoting experimental and theoretical errors, respectively. This represents a tension of 3.5 standard deviations from the combined 1σ error and is calling for new physics effects beyond the SM theory. A popular explanation for such an anomaly resides in low-scale supersymmetric models [28–38] where smuon-neutralino and sneutrino-chargino loops can explain the discrepancy (1). However, this solution is by no means unique and radiative corrections with new gauge bosons can also enhance the theoretical value of the muon anomaly such that (1) is satisfied [39]. This is indeed the case of the B-L-SM, or its SUSY version [40, 41], where a new Z' gauge boson can explain Δa_μ .

In a recent work [42], the impact of LHC searches for a light Z' boson, i.e. with mass in the range of 0.2 GeV to 200 GeV, was thoroughly investigated. In the current work, we perform a complementary study where, for heavy Z' masses beyond $m_{Z'} \gtrsim 100$ GeV, the combined effect of the electroweak precision observables and the ATLAS searches for Drell-Yan Z' production decaying into di-leptons, i.e. $pp \rightarrow Z' \rightarrow ee, \mu\mu$ [43], is investigated. We analyse whether the existing LHC constraints leave any room for explaining the $(g-2)_\mu$ anomaly and which impact it has on the model parameters and other physical observables such as the $U(1)_{B-L}$ gauge coupling g_{B-L} and the extra scalar and Z' boson masses.

The article is organized as follows. In Section II, we give a brief description of the B-L-SM structure focusing on the basic details of scalar and gauge boson mass spectra and mixing. In Section III, a detailed discussion of the numerical analysis is provided. In particular, we outline the methods and tools used in our numerical scans as well as the most relevant phenomenological constraints leading to a selection of a few representative benchmark points. Besides, the numerical results for correlations of the Z' production cross section times its branching ratio into light leptons versus the model parameters and the muon $(g-2)_\mu$ are presented. Finally, Section IV provides a short summary of our main results.

II. MODEL DESCRIPTION

In this section, we highlight the essential features of the minimal $U(1)_{B-L}$ extension of the SM relevant for our analysis. Essentially, the minimal B-L-SM is a Beyond the Standard Model (BSM) framework containing three new ingredients: 1) a new gauge interaction, 2) three generations of right handed neutrinos, and 3) a complex scalar SM-singlet. The first one is well motivated in various GUT scenarios [7–14]. However, if a family-universal symmetry such as $U(1)_{B-L}$ were introduced without changing the SM fermion content, chiral anomalies involving the $U(1)_{B-L}$ external legs would be generated. A new sector of additional three $B-L$ charged Majorana neutrinos is essential for anomaly cancellation. Also, the SM-like Higgs doublet, H , does not carry neither baryon nor lepton number, therefore does not participate in the breaking of $U(1)_{B-L}$. It is then necessary to introduce a new scalar singlet, χ , solely charged under $U(1)_{B-L}$, whose VEV breaks the $B-L$ symmetry at a scale $\langle\chi\rangle > \langle H\rangle$. It is also this breaking scale that generates masses for heavy neutrinos. The particle content and charges of the minimal $U(1)_{B-L}$ extension of the SM are summarized in Tab. I.

	$SU(3)_C$	$SU(2)_L$	$U(1)_Y$	$U(1)_{B-L}$
q_L	3	2	1/6	1/3
u_R	3	1	2/3	1/3
d_R	3	1	-1/3	1/3
ℓ_L	1	2	-1/2	-1
e_R	1	1	-1	-1
ν_R	1	1	0	-1
H	1	2	1/2	0
χ	1	1	0	2

TABLE I. Fields and their quantum numbers in the minimal B-L-SM. The last two columns represent the weak and $B-L$ hypercharges, which we denote as Y and Y_{B-L} throughout the text.

A. The scalar sector

The scalar potential of the B-L-SM reads

$$V(H, \chi) = m^2 H^\dagger H + \mu^2 \chi^* \chi + \lambda_1 (H^\dagger H)^2 + \lambda_2 (\chi^* \chi)^2 + \lambda_3 \chi^* \chi H^\dagger H \quad (2)$$

where H and χ are the Higgs doublet and the complex SM-singlet, respectively, whose real-valued components can be cast as

$$H = \frac{1}{\sqrt{2}} \begin{pmatrix} -i(\omega_1 - i\omega_2) \\ v + (h + iz) \end{pmatrix}, \quad \chi = \frac{1}{\sqrt{2}} [x + (h' + iz')]. \quad (3)$$

While v and x are the vacuum expectation values (VEVs) describing the classical ground state configurations of the theory, h and h' represent radial quantum fluctuations around the minimum of the potential. There are four Goldstone directions denoted as ω_1 , ω_2 , z and z' which are absorbed into longitudinal modes of the W , Z and Z' gauge bosons once spontaneous symmetry breaking (SSB) takes place. The scalar potential (2) is bounded from below (BFB) whenever the conditions [25]

$$4\lambda_1\lambda_2 - \lambda_3^2 > 0 \quad , \quad \lambda_1, \lambda_2 > 0 \quad . \quad (4)$$

are satisfied and the electric charge conserving vacuum

$$\langle H \rangle = \frac{1}{\sqrt{2}} \begin{pmatrix} 0 \\ v \end{pmatrix} \quad \langle \chi \rangle = \frac{x}{\sqrt{2}} \quad (5)$$

is stable. Resolving the tadpole equations with respect to the VEVs, one obtains

$$v^2 = \frac{-\lambda_2 m^2 + \frac{\lambda_3}{2} \mu^2}{\lambda_1 \lambda_2 - \frac{1}{4} \lambda_3^2} > 0 \quad \text{and} \quad x^2 = \frac{-\lambda_1 \mu^2 + \frac{\lambda_3}{2} m^2}{\lambda_1 \lambda_2 - \frac{1}{4} \lambda_3^2} > 0, \quad (6)$$

which imply, together with the BFB conditions (4), that

$$\lambda_2 m^2 < \frac{\lambda_3}{2} \mu^2 \quad \text{and} \quad \lambda_1 \mu^2 < \frac{\lambda_3}{2} m^2. \quad (7)$$

While the sign of λ_1 and λ_2 is positive, the inequalities (7) put further constraints on the signs of m^2 , μ^2 and λ_3 according to Tab. II. We see that if λ_3 is positive a minimum in the scalar potential can emerge when either μ^2 is

	$\mu^2 > 0$ $m^2 > 0$	$\mu^2 > 0$ $m^2 < 0$	$\mu^2 < 0$ $m^2 > 0$	$\mu^2 < 0$ $m^2 < 0$
$\lambda_3 < 0$	✗	✓	✓	✓
$\lambda_3 > 0$	✗	✗	✗	✓

TABLE II. Signs of parameters in the potential (2). While the ✓ symbol indicates the solutions of the tadpole conditions (7) which, together with the positively-definite scalar mass spectrum, correspond to a minimum of the scalar potential, ✗ indicates unstable configurations.

positive and m^2 negative or vice-versa. However, in our studies we have considered the solutions in the last column of Tab. II where both the $SU(2)_L$ isodoublet and the complex singlet mass parameters are negative, leaving the sign of λ_3 unconstrained.

Taking the Hessian matrix and evaluating it in the vacuum (5) one obtains

$$M^2 = \begin{pmatrix} 4\lambda_2 x^2 & \lambda_3 v x \\ \lambda_3 v x & 4\lambda_1 v^2 \end{pmatrix}, \quad (8)$$

which can be rotated to the mass eigenbasis as

$$\mathbf{m}^2 = O^\dagger_i{}^m M_{mn}^2 O^n_j = \begin{pmatrix} m_{h_1}^2 & 0 \\ 0 & m_{h_2}^2 \end{pmatrix}, \quad (9)$$

where the eigenvalues are

$$m_{h_{1,2}}^2 = \lambda_1 v^2 + \lambda_2 x^2 \mp \sqrt{(\lambda_1 v^2 - \lambda_2 x^2)^2 + (\lambda_3 x v)^2}, \quad (10)$$

and the orthogonal rotation matrix \mathbf{O} reads

$$\mathbf{O} = \begin{pmatrix} \cos \alpha_h & -\sin \alpha_h \\ \sin \alpha_h & \cos \alpha_h \end{pmatrix}. \quad (11)$$

The physical basis vectors h_1 and h_2 can then be written in terms of the gauge eigenbasis ones h and h' as follows:

$$\begin{pmatrix} h_1 \\ h_2 \end{pmatrix} = \mathbf{O} \begin{pmatrix} h \\ h' \end{pmatrix}. \quad (12)$$

In this article, we consider scenarios where $U(1)_{B-L}$ is broken above the EW-scale such that $x > v$. In the case of decoupling $v/x \ll 1$, the scalar masses and mixing angle become particularly simple,

$$\sin \alpha_h \approx \frac{1}{2} \frac{\lambda_3 v}{\lambda_2 x} \quad m_{h_1}^2 \approx 2\lambda_1 v^2 \quad m_{h_2}^2 \approx 2\lambda_2 x^2 \quad (13)$$

which represent a good approximation for most of the phenomenologically consistent points in our numerical analysis discussed below.

B. The gauge sector

The gauge boson and Higgs kinetic terms in the B-L-SM Lagrangian read

$$\mathcal{L}_{U(1)} = |D_\mu H|^2 + |D_\mu \chi|^2 - \frac{1}{4} F_{\mu\nu} F^{\mu\nu} - \frac{1}{4} F'_{\mu\nu} F'^{\mu\nu} - \frac{1}{2} \kappa F_{\mu\nu} F'^{\mu\nu}, \quad (14)$$

where $F^{\mu\nu}$ and $F'^{\mu\nu}$ are the standard $U(1)_Y$ and $U(1)_{B-L}$ field strength tensors, respectively,

$$F_{\mu\nu} = \partial_\mu A_\nu - \partial_\nu A_\mu \quad \text{and} \quad F'_{\mu\nu} = \partial_\mu A'_\nu - \partial_\nu A'_\mu. \quad (15)$$

written in terms of the gauge fields A_μ and A'_μ , respectively. The κ parameter in Eq. (14) represents the $U(1)_Y \times U(1)_{B-L}$ gauge kinetic mixing while the Abelian part of the covariant derivative reads

$$D_\mu \supset ig_1 Y A_\mu + ig'_1 Y_{B-L} A'_\mu, \quad (16)$$

with g_1 and g'_1 being the $U(1)_Y$ and $U(1)_{B-L}$ the gauge couplings, respectively, whereas the Y and $B-L$ charges are specified in Tab. I.

1. Kinetic-mixing

In order to study the kinetic mixing effects on physical observables it is convenient to rewrite the gauge kinetic terms in the canonical form, i.e.

$$F_{\mu\nu} F^{\mu\nu} + F'_{\mu\nu} F'^{\mu\nu} + 2\kappa F_{\mu\nu} F'^{\mu\nu} \rightarrow B_{\mu\nu} B^{\mu\nu} + B'_{\mu\nu} B'^{\mu\nu}. \quad (17)$$

A generic orthogonal transformation in the field space does not eliminate the kinetic mixing term. So, in order to satisfy Eq. (17) an extra non-orthogonal transformation should be imposed such that Eq. (17) is realized. Taking $\kappa = \sin \alpha$, a suitable redefinition of fields $\{A_\mu, A'_\mu\}$ into $\{B_\mu, B'_\mu\}$ that eliminates κ -term according to Eq. (14) can be cast as

$$\begin{pmatrix} A_\mu \\ A'_\mu \end{pmatrix} = \begin{pmatrix} 1 & -\tan \alpha \\ 0 & \sec \alpha \end{pmatrix} \begin{pmatrix} B_\mu \\ B'_\mu \end{pmatrix}, \quad (18)$$

such that in the limit of no kinetic-mixing, $\alpha = 0$. Note that this transformation is generic and valid for any basis in the field space. The transformation (18) results in a modification of the covariant derivative that acquires two additional terms encoding the details of the kinetic mixing, i.e.

$$D_\mu \supset \partial_\mu + i(g_Y Y + g_{BY} Y_{B-L}) B_\mu + i(g_{B-L} Y_{B-L} + g_{YB} Y) B'_\mu, \quad (19)$$

where the gauge couplings take the form

$$\begin{cases} g_Y = g_1 \\ g_{B-L} = g'_1 \sec \alpha \\ g_{YB} = -g_1 \tan \alpha \\ g_{BY} = 0 \end{cases}, \quad (20)$$

which is the standard convention in the literature. The resulting mixing between the neutral gauge fields including Z' can be represented as follows

$$\begin{pmatrix} \gamma_\mu \\ Z_\mu \\ Z'_\mu \end{pmatrix} = \begin{pmatrix} \cos \theta_W & \sin \theta_W & 0 \\ -\sin \theta_W \cos \theta'_W & \cos \theta_W \cos \theta'_W & \sin \theta'_W \\ \sin \theta_W \sin \theta'_W & -\cos \theta'_W \sin \theta'_W & \cos \theta'_W \end{pmatrix} \begin{pmatrix} B_\mu \\ A_\mu^3 \\ B'_\mu \end{pmatrix} \quad (21)$$

where θ_W is the weak mixing angle and θ'_W is defined as

$$\sin(2\theta'_W) = \frac{2g_{YB} \sqrt{g^2 + g_Y^2}}{\sqrt{(g_{YB}^2 + 16(\frac{x}{v})^2 g_{B-L}^2 - g^2 - g_Y^2)^2 + 4g_{YB}^2 (g^2 + g_Y^2)}}, \quad (22)$$

in terms of g and g_Y being the $SU(2)_L$ and $U(1)_Y$ gauge couplings, respectively. In the physically relevant limit, $v/x \ll 1$, the above expression greatly simplifies leading to

$$\sin \theta'_W \approx \frac{1}{16} \frac{g_{YB}}{g_{B-L}} \left(\frac{v}{x}\right)^2 \sqrt{g^2 + g_Y^2}, \quad (23)$$

up to $(v/x)^3$ corrections. In the limit of no kinetic mixing, i.e. $g_{YB} \rightarrow 0$, there is no mixture of Z' and SM gauge bosons.

Note, the kinetic mixing parameter θ'_W has rather stringent constraints from Z pole experiments both at the Large Electron-Positron Collider (LEP) [44] and the Stanford Linear Collider (SLC) [45], restricting its value to be smaller than 10^{-3} approximately, which we set as an upper bound in our numerical analysis. Expanding the kinetic terms $|D_\mu H|^2 + |D_\mu \chi|^2$ around the vacuum one can extract the following mass matrix for vector bosons

$$m_V^2 = \frac{v^2}{4} \begin{pmatrix} g^2 & 0 & 0 & 0 & 0 \\ 0 & g^2 & 0 & 0 & 0 \\ 0 & 0 & g^2 & -gg_Y & -gg_{YB} \\ 0 & 0 & -gg_Y & g_Y^2 & g_Y g_{YB} \\ 0 & 0 & -gg_{YB} & g_Y g_{YB} & g_{YB}^2 + 16 \left(\frac{x}{v}\right)^2 g_{B-L}^2 \end{pmatrix} \quad (24)$$

whose eigenvalues read

$$m_A = 0, \quad m_W = \frac{1}{2}vg \quad (25)$$

corresponding to physical photon and W^\pm bosons as well as

$$m_{Z,Z'} = \sqrt{g^2 + g_Y^2} \cdot \frac{v}{2} \sqrt{\frac{1}{2} \left(\frac{g_{YB}^2 + 16 \left(\frac{x}{v}\right)^2 g_{B-L}^2}{g^2 + g_Y^2} + 1 \right) \mp \frac{g_{YB}}{\sin(2\theta'_W) \sqrt{g^2 + g_Y^2}}}. \quad (26)$$

for two neutral massive vector bosons, with one of them, not necessarily the lightest, representing the SM-like Z boson. It follows from LEP and SLC constraints on θ'_W , that Eq. (23) also implies that either g_{YB} or the ratio $\frac{x}{v}$ are small. In this limit, Eq. (26) simplifies to

$$m_Z \approx \frac{1}{2}v\sqrt{g^2 + g_Y^2} \quad \text{and} \quad m_{Z'} \approx 2g_{B-L}x, \quad (27)$$

where the $m_{Z'}$ depends only on the SM-singlet VEV x and on the $U(1)_{B-L}$ gauge coupling and will be attributed to a heavy Z' state, while the light Z -boson mass corresponds to its SM value.

C. The Yukawa sector

One of the key features of the B-L-SM is the presence of non-zero neutrino masses. In its minimal version, such masses are generated via a type-I seesaw mechanism. The Yukawa Lagrangian of the model reads

$$\mathcal{L}_f = -Y_u^{ij} \bar{q}_{Li} u_{Rj} \tilde{H} - Y_d^{ij} \bar{q}_{Li} d_{Rj} H - Y_e^{ij} \bar{\ell}_{Li} e_{Rj} H - Y_\nu^{ij} \bar{\ell}_{Li} \nu_{Rj} \tilde{H} - \frac{1}{2} Y_\chi^{ij} \bar{\nu}_{Ri}^c \nu_{Rj} \chi + \text{c.c.} \quad (28)$$

Notice that Majorana neutrino mass terms of the form $M \bar{\nu}_R^c \nu_R$ would explicitly violate the $U(1)_{B-L}$ symmetry and are therefore not present. In Eq. (28), Y_u , Y_d and Y_e are the 3×3 Yukawa matrices that reproduce the quark and charged lepton sector of the SM, while Y_ν and Y_χ are the new Yukawa matrices responsible for the generation of neutrino masses and mixing. In particular, one can write

$$\mathbf{m}_{\nu_l}^{\text{Type-I}} = \frac{1}{\sqrt{2}} \frac{v^2}{x} \mathbf{Y}_\nu^\top \mathbf{Y}_\chi^{-1} \mathbf{Y}_\nu, \quad (29)$$

for light ν_l neutrino masses, whereas the heavy ν_h ones are given by

$$\mathbf{m}_{\nu_h}^{\text{Type-I}} \approx \frac{1}{\sqrt{2}} \mathbf{Y}_\chi x, \quad (30)$$

where we have assumed a flavour diagonal basis. Note that the smallness of light neutrino masses imply that either the x VEV is very large or (if we fix it to be at the $\mathcal{O}(\text{TeV})$ scale and $\mathbf{Y}_\chi \sim \mathcal{O}(1)$) the corresponding Yukawa coupling should be tiny, $\mathbf{Y}_\nu < 10^{-6}$. It is clear that the low scale character of the type-I seesaw mechanism in the minimal B-L-SM is *faked* by small Yukawa couplings to the Higgs boson. A more elegant description was proposed in Ref. [46] where small SM neutrino masses naturally result from an inverse seesaw mechanism. In this work, however, we will not study the neutrino sector and thus, for an improved efficiency of our numerical analysis of Z' observables, it will be sufficient to fix the Yukawa couplings to $\mathbf{Y}_\chi = 10^{-1}$ and $\mathbf{Y}_\nu = 10^{-7}$ values such that the three lightest neutrinos lie in the sub-eV domain.

III. PARAMETER SPACE STUDIES

To assess the phenomenological viability of the minimal B-L-SM, we have developed a scanning routine that sequentially calls publicly available software tools in order to numerically evaluate physical observables and confront them against experimental data. Analytical expressions for such observables are calculated in **SARAH 4.13.0** [47, 48] and then imported to **SPheno 4.0.3** [49, 50], which is a spectrum generator where masses and mixing angles, EW precision observables, the muon anomalous magnetic moment as well as a number of decay widths and branching fractions are numerically evaluated. Besides, various theoretical constraints such as the positivity of the one-loop mass spectrum and unitarity are taken into account. As a first step, our scanning routine randomly samples parameter space points according to the ranges in Tab. III. As can be seen from Eq. (13), λ_1 varies in a rather narrow domain

λ_1	$\lambda_{2,3}$	g_{B-L}	g_{YB}	x [TeV]
$[10^{-2}, 10^{0.5}]$	$[10^{-8}, 10]$	$[10^{-8}, 10]$	$[10^{-8}, 10]$	$[0.5, 20.5]$

TABLE III. Parameter scan ranges used in our analysis. Note that the value of λ_1 is mostly constrained by the tree-level Higgs boson mass given in Eq. (13).

in comparison to $\lambda_{2,3}$ in order to comply with the experimental data on the SM Higgs mass. In particular, provided that **SPheno** computes the SM Higgs boson mass at two-loop order, the tree-level quantity $v\sqrt{2\lambda_1}$ must not be too far from $\mathcal{O}(125 \text{ GeV})$ for most of the valid points. In fact, we have verified that valid points typically require $\lambda_1 \sim \mathcal{O}(0.12 - 0.14)$, with a few cases where quantum corrections are somewhat larger.

A. Phenomenological constraints

Each point generated with our routine undergoes a sequence of tests before being accepted. The very first layer of phenomenological checks is done by **SPheno** which promptly rejects any scenario with tachyonic scalar masses. If the positivity of squared scalar spectrum is assured, then **SPheno** verifies if unitary constraints are also fulfilled. For details see the pioneering work in [51] or the discussion in [52]. The presence of new bosons in the theory can induce large deviations in EW precision observables. Typically, the most stringent constraints emerge from the oblique S, T, U parameters [53–55], which are calculated by **SPheno**. Current precision measurements [27] provide the allowed regions

$$S = 0.02 \pm 0.10, \quad T = 0.07 \pm 0.12, \quad U = 0.00 \pm 0.09 \quad (31)$$

where S - T are 92% correlated, while S - U and T - U are -66% and -86% anti-correlated, respectively. We compare our results with the EW fit in Eq. (31) and require consistency with the best fit point within a 95% C.L. ellipsoid (see Ref. [24] for further details about this method). We show in Fig. 1 our results in the ST (left) and TU (right) planes where black points are consistent with EW precision observables at 95% C.L. whereas grey ones lie outside the corresponding ellipsoid of the best fit point and, thus, are excluded in our analysis.

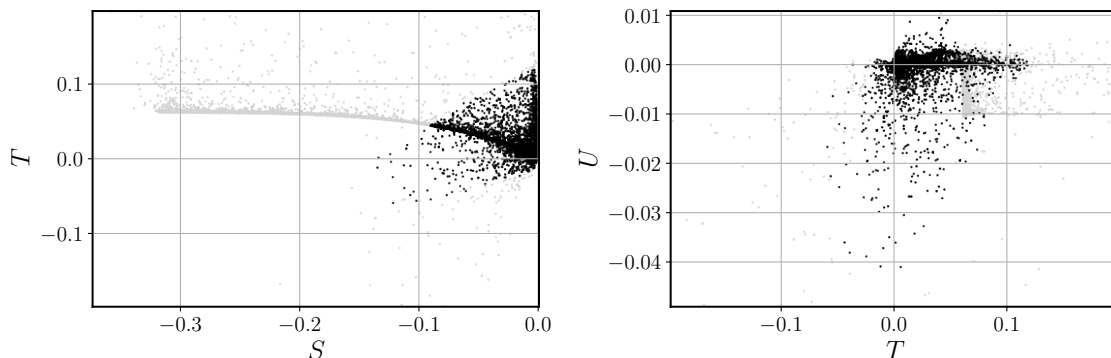


FIG. 1. Scatter plots for EW precision observables showing the ST (left) and TU (right) planes. Accepted points lying within a 95% C.L. ellipsoid of the best fit point are represented in black whereas grey points are excluded.

The B-L-SM predicts a new visible scalar, which we denote as h_2 , in addition to a SM-like 125 GeV Higgs boson, h_1 . Thus, in a second layer of phenomenological tests, we confront the surviving scenarios, black points in Fig. 1, with

collider bounds. In particular, we use `HiggsBounds 4.3.1` [56] to apply 95% C.L. exclusion limits on a new scalar particle, h_2 , and `HiggsSignals 1.4.0` [57] to check for consistency with the observed Higgs boson taking into account all known Higgs signal data. For the latter, we have accepted points whose fit to the data replicates the observed signal at 95% C.L. while the measured value for its mass, $m_{h_1} = 125.10 \pm 0.14$ GeV [27], is reproduced within a 3σ uncertainty. The required input data for `HiggsBounds/HiggsSignals` are generated by the `SPheno` output in the format of a SUSY Les Houches Accord (SLHA) [58] file. In particular, it provides scalar masses, total decay widths, Higgs decay branching ratios as well as the SM-normalized effective Higgs couplings to fermions and bosons squared (that are needed for analysis of the Higgs boson production cross sections). For details about this calculation, see Ref. [56].

On a third layer of phenomenological tests we have studied the viability of the surviving scenarios from the perspective of direct collider searches for a new Z' gauge boson. We have used `MadGraph5_aMC@NLO 2.6.2` [59] to compute the Z' Drell-Yan production cross section and subsequent decay into the first- and second-generation leptons, i.e. $\sigma(pp \rightarrow Z') \times B(Z' \rightarrow \ell\ell)$ with $\ell = e, \mu$, and then compared our results to the most recent ATLAS exclusion bounds from the LHC runs at the center-of-mass energy $\sqrt{s} = 13$ TeV [43]. The `SPheno` SLHA output files were used as parameter cards for `MadGraph5_aMC@NLO`, where the information required to calculate $\sigma(pp \rightarrow Z') \times B(Z' \rightarrow \ell\ell)$, such as the Z' boson mass, its total width and decay branching ratios into lepton pairs, is provided.

The lepton anomalous magnetic moments $(g-2)_\ell/2 \equiv a_\ell$ are calculated in `SPheno` at one-loop order. In the B-L-SM, new physics (NP) contributions to a_μ , denoted as Δa_μ^{NP} in what follows, can emerge from the diagrams containing Z' or h_2 propagators. In this article, we study whether the muon anomalous magnetic moment can be totally or partially explained in the model under consideration and all scenarios with an excessive contribution to Δa_μ^{NP} larger than the upper 2σ bound in Eq. (1) were rejected.

B. Discussion of numerical results

Let us now discuss the phenomenological properties of the B-L-SM model. First, we focus on the current collider constraints and study their impact on both the scalar and gauge sectors.

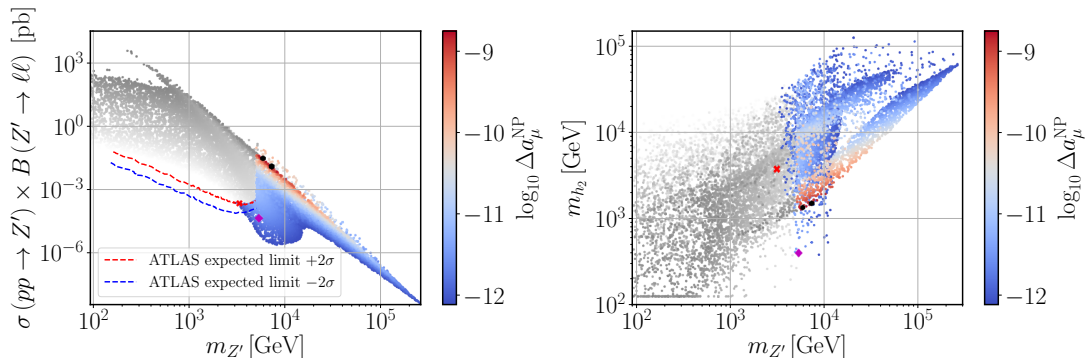


FIG. 2. Scatter plots showing the Z' Drell-Yan production cross section times the decay branching ratio into a pair of electrons and muons (left panel) and the new scalar mass m_{h_2} (right panel) as functions of $m_{Z'}$ and the new physics (NP) contributions to the muon Δa_μ anomaly. Coloured points have survived all theoretical and experimental constraints while grey points are excluded by direct Z' searches at the LHC. The region between the two dashed lines represents the current ATLAS expected limit on the production cross section times branching ratio into a pair of leptons at 95% C.L. and is taken from the *Brazilian* plot in Fig. 4 of Ref. [43]. The four highlighted points in both panels denote the benchmark scenarios described in detail in Tab. IV.

We show in Fig. 2 the scenarios generated in our parameter space scan (see Tab. III) that have passed all theoretical constraints such as boundedness from below, unitarity and EW precision tests, are compatible with the SM Higgs data and where a new visible scalar h_2 is unconstrained by the direct collider searches. On the left panel, we show the Z' production cross section times its branching ratio to the first- and second-generation leptons, $\sigma B \equiv \sigma(pp \rightarrow Z') \times B(Z' \rightarrow \ell\ell)$ with $\ell = e, \mu$, as a function of the new vector boson mass and the new physics contribution to the muon anomalous magnetic moment Δa_μ^{NP} (colour scale). On the right panel, we show the new scalar mass as a function of the same observables. All points above the red dashed line are excluded at 95% C.L. by the upper expected limit on Z' direct searches at the LHC by the ATLAS experiment and are represented in grey shades. Darker shades denote *would-be-scenarios* with larger values of Δa_μ^{NP} while the smaller contributions to the muon $(g-2)_\mu/2$

anomaly are represented with the lighter shades. The region between the two dashed lines corresponds to the Z' ATLAS limit with a 2σ uncertainty represented by the yellow band in Fig. 4 of [43]. Provided that the observed limit by the ATLAS detector lies within this region we have taken a conservative approach and accepted all points whose σB value lies below the red dashed line (upper limit) in Fig. 2. The blue dashed line, which corresponds to the stricter 2σ lower bound, is only shown for completeness of information. The red cross in our figures signals the lightest Z' found in our scan which we regard as a possible early-discovery (or early-exclusion) benchmark point in the forthcoming LHC runs. Such a benchmark point is shown in the first line of Tab. IV. On the right panel, we notice that the new scalar bosons can become as light as 380–400 GeV, but with Z' masses in the range of 5–9 TeV. We highlight with a magenta diamond the benchmark point with the lightest Z' boson within this range. This point is shown in the second line of Tab. IV.

$m_{Z'}$	m_{h_2}	x	$\log_{10} \Delta a_\mu^{\text{NP}}$	σB	θ'_W	α_h	$g_{\text{B-L}} \simeq g^{\ell\ell Z'}$
3.13	3.72	15.7	-12.1	2.22×10^{-4}	≈ 0	5.67×10^{-5}	0.0976
5.37	0.396	9.10	-11.7	4.23×10^{-5}	2.55×10^{-7}	9.44×10^{-7}	0.302
7.35	1.49	0.321	-8.75	0.0115	1.83×10^{-7}	1.20×10^{-6}	3.15
5.91	1.32	0.335	-8.78	0.0285	1.30×10^{-4}	1.04×10^{-5}	2.94

TABLE IV. A selection of four benchmark points represented in Figs. 2, 4 to 6. The $m_{Z'}$, m_{h_2} and x parameters are given in TeV. The first line represents a point with light h_2 while the second line shows the lightest allowed Z' boson found in our scan. The last two lines show two points that reproduce the observed value of the muon $(g-2)_\mu$ within 1σ uncertainty.

1. Implications of direct Z' searches at the LHC for the $(g-2)_\mu$ anomaly

Looking again to Fig. 2 (left panel), we see that there is a thin dark-red stripe where Δa_μ^{NP} explains the observed anomaly shown in Eq. (1) for a range of $m_{Z'}$ boson masses approximately between 5 TeV and 20 TeV. This region is particularly interesting as it can be partially probed by the forthcoming LHC runs or at future colliders. If a Z' boson discovery remains elusive for such a mass range, it can exclude a possibility of explaining the muon $(g-2)_\mu$ anomaly in the context of the B-L-SM. It is also worth noticing that such preferred Δa_μ^{NP} values represent a small island in the right plot of Fig. 2 where the new scalar boson mass is restricted to the range of $1 \text{ TeV} < m_{h_2} < 4 \text{ TeV}$.

New physics contributions Δa_μ^{NP} to the muon anomalous magnetic moment are given at one-loop order by the Feynman diagrams depicted in Fig. 3. Since the couplings of a new scalar h_2 to the SM fermions are suppressed by a

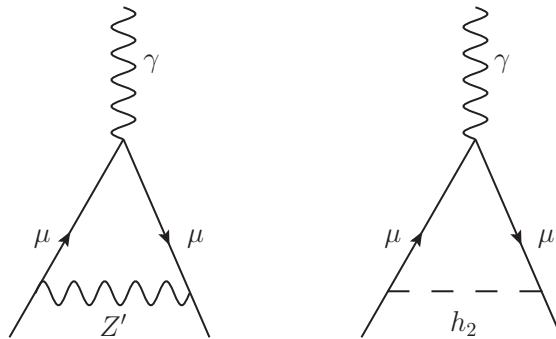


FIG. 3. One-loop diagrams contributing to Δa_μ^{NP} in the B-L-SM.

factor of $\sin \alpha_h$, which we find to be always smaller than 0.08 as can be seen in the bottom panel of Fig. 4, the right diagram in Fig. 3, which scales as $\Delta a_\mu^{h_2} \propto \frac{m_\mu^2}{m_{h_2}^2} (y_\mu \sin \alpha_h)^2$ with $\sin^2 \alpha_h < 0.0064$ and $y_\mu = Y_e^{22}$, provides sub-leading contributions to Δa_μ . Furthermore, as we show in the top-left panel of Fig. 4 the new scalar boson mass, which we have found to satisfy $m_{h_2} \gtrsim 380 \text{ GeV}$, is not light enough to compensate the smallness of the scalar mixing angle. Conversely, and recalling that all fermions in the B-L-SM transform non-trivially under $U(1)_{\text{B-L}}$, the new Z' boson

can have sizeable couplings to fermions via gauge interactions proportional to g_{B-L} . Therefore, the left diagram in Fig. 3 provides the leading contribution to the $(g-2)_\mu$ in the model under consideration. In particular, $\Delta a_\mu^{Z'}$ is given

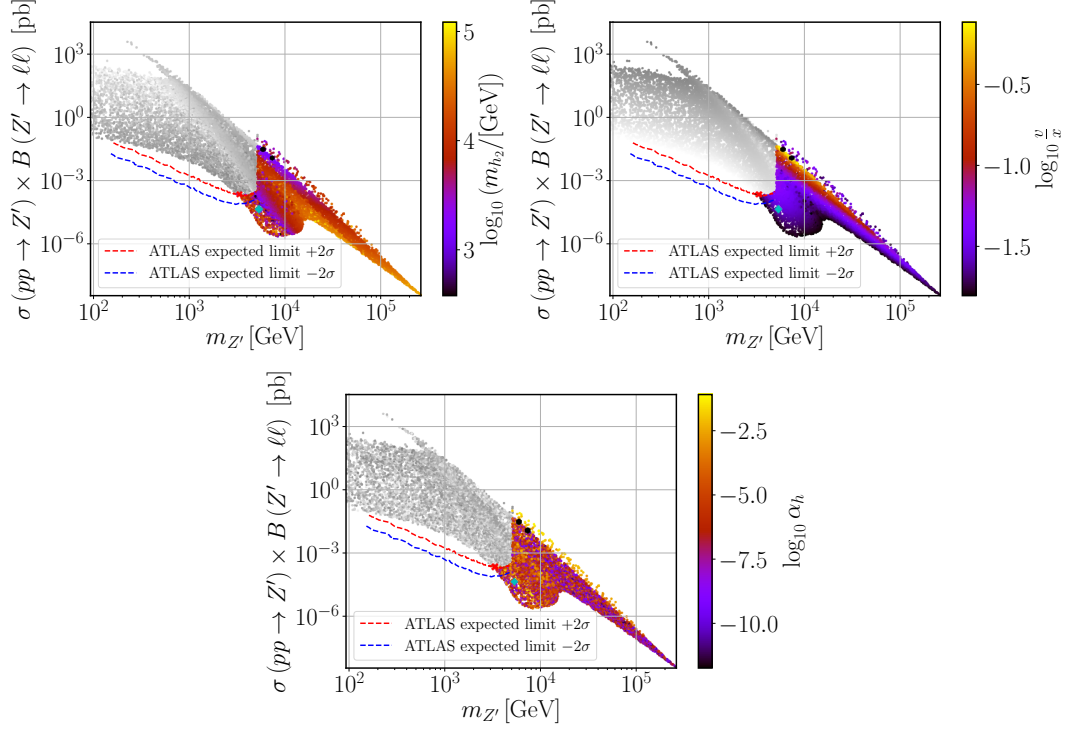


FIG. 4. Scatter plots showing the Z' Drell-Yan production cross section times the decay branching ratio into a pair of electrons and muons in terms of the $m_{Z'}$ boson mass. The colour gradation represents the new scalar mass (top-left), the ratio between the EW- and $U(1)_{B-L}$ -breaking VEVs (top-right) and the scalar mixing angle (bottom). The grey points are excluded by direct Z' searches at the LHC. The four benchmark points in Tab. IV are represented by the black dots (last two rows), cyan diamond (first row) and red cross (second row).

by [60]

$$\Delta a_\mu^{Z'} = \frac{1}{12\pi^2} \frac{m_\mu^2}{m_{Z'}^2} \left(3g_L^{\mu\mu Z'} g_R^{\mu\mu Z'} - g_L^{\mu\mu Z'^2} - g_R^{\mu\mu Z'^2} \right) \quad (32)$$

where the left- and right-chiral projections of the charged lepton couplings to the Z' boson, $g_L^{\ell\ell Z'}$ and $g_R^{\ell\ell Z'}$, respectively, can be approximated as follows

$$\begin{aligned} g_L^{\ell\ell Z'} &\simeq g_{B-L} + \frac{1}{32} \left(\frac{v}{x} \right)^2 \frac{g_{YB}}{g_{B-L}} [g_Y^2 - g^2 + 2g_Y g_{YB}], \\ g_R^{\ell\ell Z'} &\simeq g_{B-L} + \frac{1}{16} \left(\frac{v}{x} \right)^2 \frac{g_{YB}}{g_{B-L}} [g_Y^2 + g_Y g_{YB}], \end{aligned} \quad (33)$$

to the second order in v/x -expansion. If $v/x \ll 1$, corresponding to the darker shades of the color scale in the top-right panel of Fig. 4, we can further approximate

$$g_L^{\ell\ell Z'} \simeq g_R^{\ell\ell Z'} \simeq g_{B-L}, \quad (34)$$

such that the muon anomalous magnetic moment gets significantly simplified to

$$\Delta a_\mu^{Z'} \simeq \frac{g_{B-L}^2}{12\pi^2} \frac{m_\mu^2}{m_{Z'}^2}. \quad (35)$$

Similarly, for the yellow band, which corresponds to the region where Δa_μ^{NP} is maximized (see top-left panel of Fig. 2), a large value of the $U(1)_{B-L}$ gauge coupling also allows one to simplify Eq. (32) reducing it to the form of Eq. (35).

This is in fact what we have observed and, for the yellow band region, we see in the bottom panel of Fig. 5 that $g_{B-L} \simeq 3$. A sizeable value of g_{B-L} is indeed what is contributing to the enhancement of Δa_μ^{NP} , in particular, for the red region in both panels of Fig. 2. We show in the third and fourth lines of Tab. IV the two benchmark points that better reproduce the muon anomalous moment represented by two black dots in Figs. 2, 4 to 6.

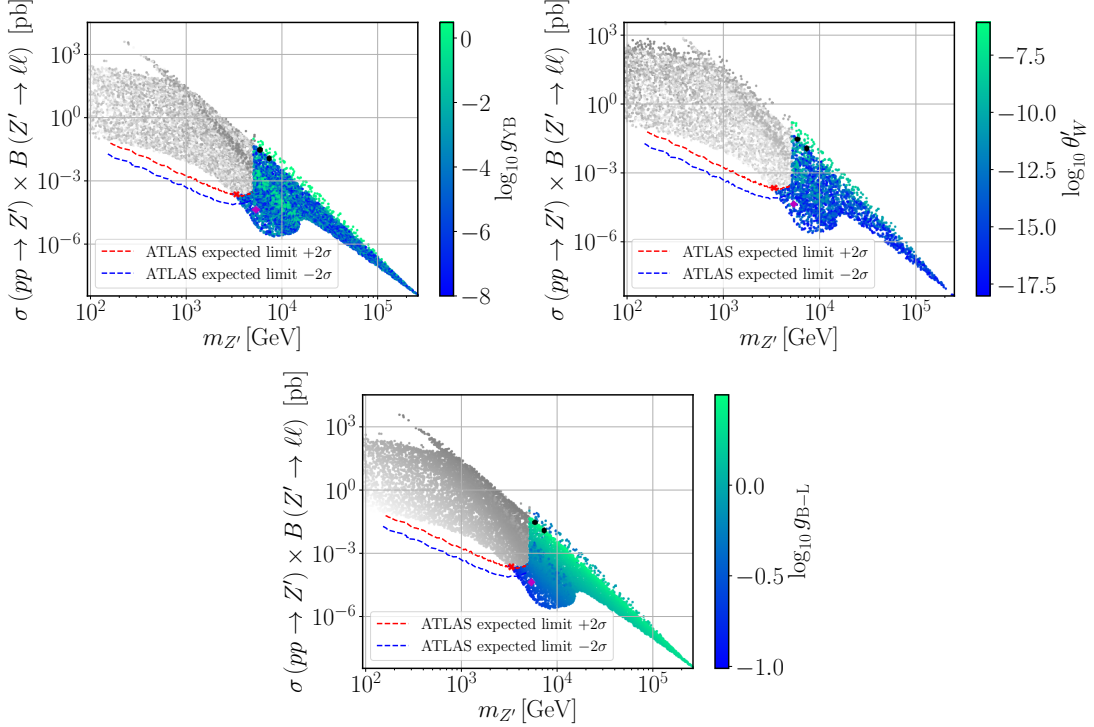


FIG. 5. The same as in Fig. 4 but with the colour scale representing the gauge-mixing parameters g_{YB} (top-left) and θ'_W (top-right), and the $U(1)_{B-L}$ gauge coupling (bottom).

In fact, a close inspection of Fig. 2 (left panel) and Fig. 4 (top-right panel) reveals an almost one-to-one correspondence between the colour shades. This suggests that $\Delta a_\mu^{Z'}$ must somehow be related to the VEV ratio v/x . To understand this behaviour, let us also look to Fig. 5 (top-right panel) where we see that the kinetic-mixing gauge coupling g_{YB} is typically very small apart from two green bands where it can become of order $\mathcal{O}(1)$. Interestingly, whenever g_{YB} becomes sizeable, $v/x \ll 1$ is realised, which means that Eq. (27) is indeed a good approximation as was argued above. It is then possible to eliminate g_{B-L} from Eq. (35) and rewrite it as

$$\Delta a_\mu^{Z'} \simeq \frac{y_\mu^2}{96\pi^2} \left(\frac{v}{x}\right)^2, \quad (36)$$

which explains the observed correlation between both Fig. 2 (left panel) and Fig. 4 (top-right panel) and, for instance, the thin red stripe of points compatible with a full description of the muon $(g-2)_\mu/2$ anomaly. Note that this simple and illuminating relation becomes valid as a consequence of the heavy Z' mass regime, in combination with the smallness of the θ'_W mixing angle required by LEP constraints. Indeed, while we have not imposed any strong restriction on the input parameters of our scan (see Tab. III), Eq. (23) necessarily implies that both g_{YB} and v/x cannot be simultaneously sizeable in agreement with what is seen in Fig. 5 (top-left panel) and Fig. 4 (top-right panel). The values of θ'_W obtained in our scan are shown in the top-right panel of Fig. 5.

For completeness, we show in Fig. 6 the physical couplings of Z' to muons (top panels) and to W^\pm bosons (bottom panel). Note that, for the considered scenarios, the latter can be written as

$$g^{WWZ'} \simeq \frac{1}{16} \frac{g_{YB}}{g_{B-L}} \left(\frac{v}{x}\right)^2. \quad (37)$$

While both g_{B-L} and the ratio v/x provide a smooth continuous contribution in the $\sigma B - m_{Z'}$ projection of the parameter space, the observed blurry region in $g^{WWZ'}$ is correlated with the one in the top-left panel of Fig. 5 as expected from Eq. (37). On the other hand, the couplings to leptons $g_{L,R}^{\ell\ell Z'}$ exhibit a strong correlation with g_{B-L} in Fig. 5, in agreement with our discussion above and with Eq. (34).

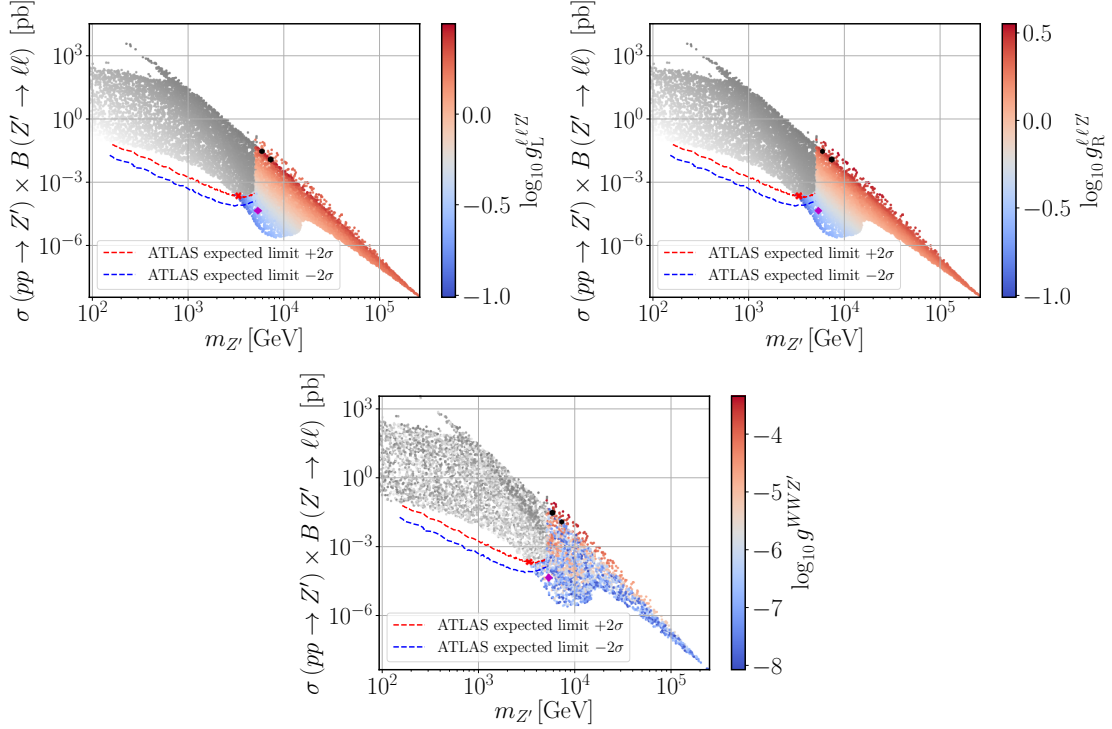


FIG. 6. The same as in Fig. 4 but with the colour scale representing the coupling of leptons to the Z' (top panels) and the coupling of W bosons to Z' .

2. Barr-Zee type contributions

To conclude our analysis, one should note that the two-loop Barr-Zee type diagrams [61] are always sub-dominant in our case. To see this, let us consider the four diagrams shown in Fig. 7. The same reason that suppresses the one-loop h_2 contribution in Fig. 3 is also responsible for the suppression of both the top-right and bottom-right diagrams in Fig. 7 (for details see e.g. Ref. [62]). Recall that the coupling of h_2 to the SM particles is proportional to the scalar mixing angle α_h , which is always small (or very small) as we can see in Fig. 4. An analogous effect is present in the diagram involving a W -loop, where a vertex proportional to $g^{WWZ'}$ suppresses such a contribution. The only diagram that might play a sizeable role is the top-left one where the couplings of Z' to both muons and top quarks are not negligible.

Let us then estimate the size of the first diagram in Fig. 7. This type of diagrams were already calculated in Ref. [63] but for the case of a SM Z -boson. Since the same topology holds for the considered case of B-L-SM too, if we trade Z by the new Z' boson, the contribution to the muon $(g-2)_\mu$ anomaly can be rewritten as

$$\Delta a_\mu^{\gamma Z'} = -\frac{g^2 g_{\text{B-L}}^2 m_\mu^2 \tan^2 \theta_W}{1536\pi^4} \left(g_L^{ttZ'} - g_R^{ttZ'} \right) \text{T}_7(m_{Z'}^2, m_t^2, m_t^2), \quad (38)$$

where $g_{\text{L,R}}^{ttZ'}$, calculated in SARAH, are the left- and right-chirality projections of the Z' coupling to top-quarks, given by

$$\begin{aligned} g_L^{ttZ'} &= -\frac{g_{\text{B-L}}}{3} \cos \theta'_W + \frac{g}{2} \cos \theta_W \sin \theta'_W - \frac{g_Y}{6} \sin \theta_W \sin \theta'_W - \frac{g_{\text{YB}}}{3} \sin \theta_W \sin \theta'_W, \\ g_R^{ttZ'} &= -\frac{g_{\text{B-L}}}{3} \cos \theta'_W - \frac{2g_Y}{3} \sin \theta_W \sin \theta'_W - \frac{g_{\text{YB}}}{3} \sin \theta_W \sin \theta'_W. \end{aligned} \quad (39)$$

The loop integral $\text{T}_7(m_{Z'}^2, m_t^2, m_t^2)$ was determined in Ref. [63] and, in the limit $m_{Z'} \gg m_t$, as we show in Eq. (A8), it gets simplified to

$$\text{T}_7(m_{Z'}^2, m_t^2, m_t^2) \simeq \frac{2}{m_{Z'}^2}, \quad (40)$$

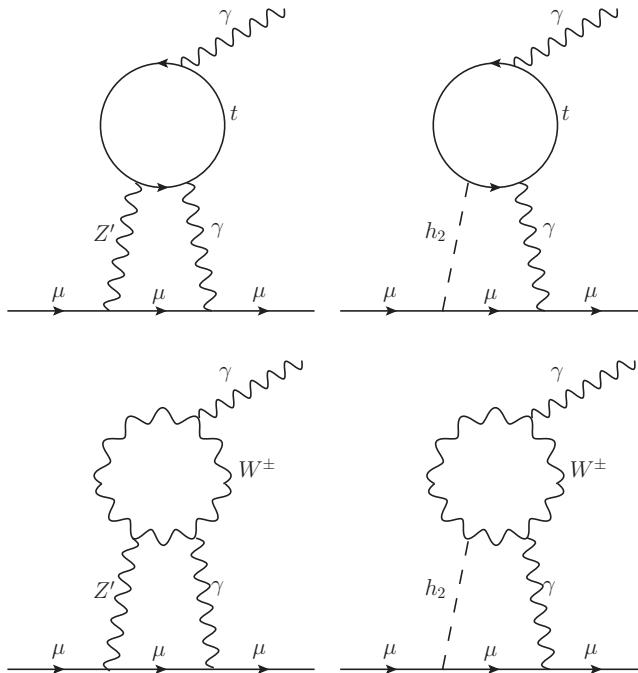


FIG. 7. Barr-Zee type two-loop diagrams contributing to Δa_μ .

up to a small truncation error (see Appendix A for details). For the parameter space region under consideration the difference $g_L^{ttZ'} - g_R^{ttZ'}$ can be cast in a simplified form as follows

$$\left(g_L^{ttZ'} - g_R^{ttZ'}\right) \simeq \frac{(g^2 + g_Y^2) g_{YB}}{32g_{B-L}} \left(\frac{v}{x}\right)^2. \quad (41)$$

Using this result and the approximate value of the loop factor, we can calculate the ratio between the two- and one-loop contributions to the muon $(g - 2)_\mu$,

$$\frac{\Delta a_\mu^{\gamma Z'}}{\Delta a_\mu^{Z'}} \simeq -\frac{g^2 g_Y^2 g_{YB}}{2048\pi^2 g_{B-L}} \left(\frac{v}{x}\right)^2 \ll 1, \quad (42)$$

which shows that $\Delta a_\mu^{\gamma Z'}$ does indeed play a subdominant role in our analysis and can be safely neglected.

IV. CONCLUSION

To summarise, in this work we have performed a detailed phenomenological analysis of the minimal $U(1)_{B-L}$ extension of the Standard Model known as the B-L-SM. In particular, we have confronted the model with the most recent experimental bounds from the direct Z' boson and next-to-lightest Higgs state searches at the LHC. Simultaneously, we have analysed the prospects of the B-L-SM for a consistent explanation of the observed anomaly in the muon anomalous magnetic moment $(g - 2)_\mu$. For this purpose, we have explored the B-L-SM potential for interpretation of the $(g - 2)_\mu$ anomaly in the regions of the model parameter space that are consistent with direct searches and electroweak precision observables.

As one of the main results of our analysis, we have found phenomenologically consistent model parameter space regions that simultaneously fit the exclusion limits from direct Z' searches and can explain the muon $(g - 2)_\mu$ anomaly. In particular, we have identified four benchmark points for future phenomenological exploration – the first one with the lightest Z' ($m_{Z'} > 3.1$ TeV), the second – with the lightest second scalar boson ($m_{h_2} > 400$ GeV), and the other two points that reproduce the muon $(g - 2)_\mu$ anomaly within 1σ uncertainty range. Besides, we have studied the correlations of the Z' production cross section times the branching ratio into a pair of light leptons versus the physical parameters of the model. In particular, we have found that the muon $(g - 2)_\mu$ observable dominated by Z' loop contributions lies within the phenomenologically viable parameter space domain. For completeness, we have also estimated the dominant contribution from the Barr-Zee type two-loop corrections and found a relatively small effect.

ACKNOWLEDGMENTS

The authors would like to thank Werner Porod and Florian Staub for discussions on the **SPheno** implementation of the muon $(g-2)_\mu$. The authors would also like to thank Nuno Castro and Maria Ramos for insightful discussions about the implementation of the current model in **MadGraph5_aMC@NLO**. J.P.R thanks Lund University for hospitality during a short and fruitful visit. The work of A.P.M. has been performed in the framework of COST Action CA16201 ‘‘Unraveling new physics at the LHC through the precision frontier’’ (PARTICLEFACE). A.P.M. is supported by Fundaao para a Ciencia e a Tecnologia (FCT), within project UID/MAT/04106/2019 (CIDMA) and by national funds (OE), through FCT, I.P., in the scope of the framework contract foreseen in the numbers 4, 5 and 6 of the article 23, of the Decree-Law 57/2016, of August 29, changed by Law 57/2017, of July 19. A.P.M. is also supported by the *Enabling Green E-science for the Square Kilometer Array Research Infrastructure* (ENGAGESKA), POCI-01-0145-FEDER-022217. A.P.M. and J.P.R are supported by the project *From Higgs Phenomenology to the Unification of Fundamental Interactions*, PTDC/FIS-PAR/31000/2017. R.P. is partially supported by the Swedish Research Council, contract number 621-2013-428.

Appendix A: The loop integral $T_7(x, y, x)$

In Appendix B of Ref. [63], the exact integral equations for $T_7(x, y, z)$ are provided. In our analysis we consider the limit where $x \gg y = z$, with $x = m_Z^2$, and $y = z = m_t^2$, where Eq. (40) provides a good approximation up to a truncation error. Here, we show the main steps in determining Eq. (40). The exact form of the loop integral reads as

$$\begin{aligned} T_7(x, y, y) = & -\frac{1}{x^2}\varphi_0(y, y) + 2y\frac{\partial^3\Phi(x, y, y)}{\partial x\partial y^2} + \frac{\partial^2\Phi(x, y, y)}{\partial x^2} + x\frac{\partial^3\Phi(x, y, y)}{\partial x^2\partial y} \\ & + \frac{\Phi(x, y, y)}{x^2} - \frac{1}{x}\frac{\partial\Phi(x, y, y)}{\partial x} + \frac{\partial^2\Phi(x, y, y)}{\partial x\partial y}, \end{aligned} \quad (\text{A1})$$

with $\varphi_0(x, y)$ and $\Phi(x, y, z)$ defined in Ref. [63]. Let us now expand each of the terms for $x \ll y$. While the first term is exact and has the form

$$-\frac{1}{x^2}\varphi_0(y, y) = -2\frac{y}{x^2}\log^2 y, \quad (\text{A2})$$

the second can be approximated to

$$2y\frac{\partial^3\Phi(x, y, y)}{\partial x\partial y^2} \simeq \xi\frac{24}{x} = \frac{8}{x} \text{ for } \xi = \frac{1}{3}. \quad (\text{A3})$$

In Eq. (A3), the $\xi = \frac{1}{3}$ factor was introduced in order to compensate for a truncation error. This was obtained by comparing the numerical values of the exact expression and our approximation. The third term can be simplified to

$$\frac{\partial^2\Phi(x, y, y)}{\partial x^2} \simeq \frac{2}{x}\left(\log y - \log\frac{y}{x}\right) + \frac{2}{x}, \quad (\text{A4})$$

and the fourth to

$$x\frac{\partial^3\Phi(x, y, y)}{\partial x^2\partial y} \simeq -\frac{4}{x}\left(\log\frac{y}{x} + 1\right). \quad (\text{A5})$$

The fifth and the seventh terms read

$$\frac{\Phi(x, y, y)}{x^2} - \frac{1}{x}\frac{\partial\Phi(x, y, y)}{\partial x} \simeq \frac{2}{x}\log\frac{1}{x}, \quad (\text{A6})$$

and finally, the sixth terms can be expanded as

$$\frac{\partial^2\Phi(x, y, y)}{\partial x\partial y} \simeq \frac{4}{x}\left(\log\frac{y}{x} - 1\right). \quad (\text{A7})$$

Noting that Eq. (A2) is of the order $\frac{1}{x^2}$, putting together Eqs. (A1), (A3), (A4), (A5), (A6), and (A7) we get for the leading $\frac{1}{x}$ contributions the following:

$$T_7(x, y, y) \simeq \overbrace{\frac{2}{x}\left(\log y - \log\frac{y}{x}\right) + \frac{2}{x}\log\frac{1}{x}}^0 - \overbrace{\frac{4}{x}\left(\log\frac{y}{x} + 1\right) + \frac{4}{x}\left(\log\frac{y}{x} - 1\right) + \frac{8}{x} + \frac{2}{x}}^{-\frac{8}{x}} \simeq \frac{2}{x}. \quad (\text{A8})$$

-
- [1] Tsutomu Yanagida, “Horizontal gauge symmetry and masses of neutrinos,” *Proceedings: Workshop on the Unified Theories and the Baryon Number in the Universe: Tsukuba, Japan, February 13-14, 1979*, Conf. Proc. **C7902131**, 95–99 (1979).
- [2] Murray Gell-Mann, Pierre Ramond, and Richard Slansky, “Complex Spinors and Unified Theories,” *Supergravity Workshop Stony Brook, New York, September 27-28, 1979*, Conf. Proc. **C790927**, 315–321 (1979), arXiv:1306.4669 [hep-th].
- [3] Rabindra N. Mohapatra and Goran Senjanovic, “Neutrino Mass and Spontaneous Parity Nonconservation,” *Phys. Rev. Lett.* **44**, 912 (1980), [231(1979)].
- [4] Rabindra N. Mohapatra and R. E. Marshak, “Local B-L Symmetry of Electroweak Interactions, Majorana Neutrinos and Neutron Oscillations,” *Phys. Rev. Lett.* **44**, 1316–1319 (1980), [Erratum: *Phys. Rev. Lett.* **44**, 1643(1980)].
- [5] Lorenzo Basso, Stefano Moretti, and Giovanni Marco Pruna, “Constraining the g'_1 coupling in the minimal $B-L$ Model,” *J. Phys.* **G39**, 025004 (2012), arXiv:1009.4164 [hep-ph].
- [6] Lorenzo Basso, Stefano Moretti, and Giovanni Marco Pruna, “Theoretical constraints on the couplings of non-exotic minimal Z' bosons,” *JHEP* **08**, 122 (2011), arXiv:1106.4762 [hep-ph].
- [7] Michael S. Chanowitz, John R. Ellis, and Mary K. Gaillard, “The Price of Natural Flavor Conservation in Neutral Weak Interactions,” *Nucl. Phys.* **B128**, 506–536 (1977).
- [8] Harald Fritzsch and Peter Minkowski, “Unified Interactions of Leptons and Hadrons,” *Annals Phys.* **93**, 193–266 (1975).
- [9] Howard Georgi and Dimitri V. Nanopoulos, “T Quark Mass in a Superunified Theory,” *Phys. Lett.* **82B**, 392–394 (1979).
- [10] Howard Georgi and Dimitri V. Nanopoulos, “Ordinary Predictions from Grand Principles: T Quark Mass in $O(10)$,” *Nucl. Phys.* **B155**, 52–74 (1979).
- [11] Howard Georgi and Dimitri V. Nanopoulos, “Masses and Mixing in Unified Theories,” *Nucl. Phys.* **B159**, 16–28 (1979).
- [12] Yoav Achiman and Berthold Stech, “Quark Lepton Symmetry and Mass Scales in an E6 Unified Gauge Model,” *Phys. Lett.* **77B**, 389–393 (1978).
- [13] F. Gursev, Pierre Ramond, and P. Sikivie, “A Universal Gauge Theory Model Based on E6,” *Phys. Lett.* **60B**, 177–180 (1976).
- [14] Feza Gursev and Meral Serdaroglu, “E6 GAUGE FIELD THEORY MODEL REVISITED,” *10th International Colloquium: Group Theoretical Methods in Physics Canterbury, England, August 31-September 4, 1981*, *Nuovo Cim.* **A65**, 337 (1981), [271(1981)].
- [15] Kunio Kaneta, Zhaofeng Kang, and Hye-Sung Lee, “Right-handed neutrino dark matter under the $B-L$ gauge interaction,” *JHEP* **02**, 031 (2017), arXiv:1606.09317 [hep-ph].
- [16] Nobuchika Okada and Osamu Seto, “Higgs portal dark matter in the minimal gauged $U(1)_{B-L}$ model,” *Phys. Rev.* **D82**, 023507 (2010), arXiv:1002.2525 [hep-ph].
- [17] Satomi Okada, “ Z' Portal Dark Matter in the Minimal $B-L$ Model,” *Adv. High Energy Phys.* **2018**, 5340935 (2018), arXiv:1803.06793 [hep-ph].
- [18] M. Fukugita and T. Yanagida, “Baryogenesis Without Grand Unification,” *Phys. Lett.* **B174**, 45–47 (1986).
- [19] Apostolos Pilaftsis, “CP violation and baryogenesis due to heavy Majorana neutrinos,” *Phys. Rev.* **D56**, 5431–5451 (1997), arXiv:hep-ph/9707235 [hep-ph].
- [20] Apostolos Pilaftsis and Thomas E. J. Underwood, “Resonant leptogenesis,” *Nucl. Phys.* **B692**, 303–345 (2004), arXiv:hep-ph/0309342 [hep-ph].
- [21] Giuseppe Degrandi, Stefano Di Vita, Joan Elias-Miro, Jose R. Espinosa, Gian F. Giudice, Gino Isidori, and Alessandro Strumia, “Higgs mass and vacuum stability in the Standard Model at NNLO,” *JHEP* **08**, 098 (2012), arXiv:1205.6497 [hep-ph].
- [22] S. Alekhin, A. Djouadi, and S. Moch, “The top quark and Higgs boson masses and the stability of the electroweak vacuum,” *Phys. Lett.* **B716**, 214–219 (2012), arXiv:1207.0980 [hep-ph].
- [23] Dario Buttazzo, Giuseppe Degrandi, Pier Paolo Giardino, Gian F. Giudice, Filippo Sala, Alberto Salvio, and Alessandro Strumia, “Investigating the near-criticality of the Higgs boson,” *JHEP* **12**, 089 (2013), arXiv:1307.3536 [hep-ph].
- [24] Raul Costa, Antnio P. Morais, Marco O. P. Sampaio, and Rui Santos, “Two-loop stability of a complex singlet extended Standard Model,” *Phys. Rev.* **D92**, 025024 (2015), arXiv:1411.4048 [hep-ph].
- [25] Lorenzo Basso, Stefano Moretti, and Giovanni Marco Pruna, “A Renormalisation Group Equation Study of the Scalar Sector of the Minimal B-L Extension of the Standard Model,” *Phys. Rev.* **D82**, 055018 (2010), arXiv:1004.3039 [hep-ph].
- [26] Vernon Barger, Paul Langacker, Mathew McCaskey, Michael Ramsey-Musolf, and Gabe Shaughnessy, “Complex Singlet Extension of the Standard Model,” *Phys. Rev.* **D79**, 015018 (2009), arXiv:0811.0393 [hep-ph].
- [27] M. Tanabashi *et al.* (Particle Data Group), “Review of Particle Physics,” *Phys. Rev.* **D98**, 030001 (2018).
- [28] Alexander S. Belyaev, Jose E. Camargo-Molina, Steve F. King, David J. Miller, Antnio P. Morais, and Patrick B. Schaefer, “A to Z of the Muon Anomalous Magnetic Moment in the MSSM with Pati-Salam at the GUT scale,” *JHEP* **06**, 142 (2016), arXiv:1605.02072 [hep-ph].
- [29] J. A. Grifols and A. Mendez, “Constraints on Supersymmetric Particle Masses From $(g-2)_\mu$,” *Phys. Rev.* **D26**, 1809 (1982).
- [30] John R. Ellis, John S. Hagelin, and Dimitri V. Nanopoulos, “Spin 0 Leptons and the Anomalous Magnetic Moment of the Muon,” *Phys. Lett.* **116B**, 283–286 (1982).
- [31] David A. Kosower, Lawrence M. Krauss, and Norisuke Sakai, “Low-Energy Supergravity and the Anomalous Magnetic Moment of the Muon,” *Phys. Lett.* **133B**, 305–310 (1983).

- [32] T. C. Yuan, Richard L. Arnowitt, Ali H. Chamseddine, and Pran Nath, “Supersymmetric Electroweak Effects on $G-2$ (μ),” *Z. Phys.* **C26**, 407 (1984).
- [33] J. C. Romao, A. Barroso, M. C. Bento, and G. C. Branco, “Flavor Violation in Supersymmetric Theories,” *Nucl. Phys.* **B250**, 295–311 (1985).
- [34] Gi-Chol Cho, Kaoru Hagiwara, Yu Matsumoto, and Daisuke Nomura, “The MSSM confronts the precision electroweak data and the muon $g-2$,” *JHEP* **11**, 068 (2011), arXiv:1104.1769 [hep-ph].
- [35] Nobuchika Okada, Shabbar Raza, and Qaisar Shafi, “Particle Spectroscopy of Supersymmetric SU(5) in Light of 125 GeV Higgs and Muon $g-2$ Data,” *Phys. Rev.* **D90**, 015020 (2014), arXiv:1307.0461 [hep-ph].
- [36] Motoi Endo, Koichi Hamaguchi, Teppei Kitahara, and Takahiro Yoshinaga, “Probing Bino contribution to muon $g-2$,” *JHEP* **11**, 013 (2013), arXiv:1309.3065 [hep-ph].
- [37] Iliia Gogoladze, Fariha Nasir, Qaisar Shafi, and Cem Salih Un, “Nonuniversal Gaugino Masses and Muon $g-2$,” *Phys. Rev.* **D90**, 035008 (2014), arXiv:1403.2337 [hep-ph].
- [38] Fei Wang, Wenyu Wang, and Jin Min Yang, “Reconcile muon $g-2$ anomaly with LHC data in SUGRA with generalized gravity mediation,” *JHEP* **06**, 079 (2015), arXiv:1504.00505 [hep-ph].
- [39] Andrzej Czarnecki and William J. Marciano, “The Muon anomalous magnetic moment: A Harbinger for ‘new physics’,” *Phys. Rev.* **D64**, 013014 (2001), arXiv:hep-ph/0102122 [hep-ph].
- [40] Shaaban Khalil and Cem Salih Un, “Muon Anomalous Magnetic Moment in SUSY B-L Model with Inverse Seesaw,” *Phys. Lett.* **B763**, 164–168 (2016), arXiv:1509.05391 [hep-ph].
- [41] Jin-Lai Yang, Tai-Fu Feng, Yu-Li Yan, Wei Li, Shu-Min Zhao, and Hai-Bin Zhang, “Lepton-flavor violation and two loop electroweak corrections to $(g-2)_\mu$ in the B-L symmetric SSM,” *Phys. Rev.* **D99**, 015002 (2019), arXiv:1812.03860 [hep-ph].
- [42] Frank F. Deppisch, Suchita Kulkarni, and Wei Liu, “Searching for a light Z' through Higgs production at the LHC,” *Phys. Rev.* **D100**, 115023 (2019), arXiv:1908.11741 [hep-ph].
- [43] Morad Aaboud *et al.* (ATLAS), “Search for new high-mass phenomena in the dilepton final state using 36 fb^{-1} of proton-proton collision data at $\sqrt{s} = 13 \text{ TeV}$ with the ATLAS detector,” *JHEP* **10**, 182 (2017), arXiv:1707.02424 [hep-ex].
- [44] S. Schael *et al.* (ALEPH, DELPHI, L3, OPAL, SLD, LEP Electroweak Working Group, SLD Electroweak Group, SLD Heavy Flavour Group), “Precision electroweak measurements on the Z resonance,” *Phys. Rept.* **427**, 257–454 (2006), arXiv:hep-ex/0509008 [hep-ex].
- [45] T. Aaltonen *et al.* (CDF), “Search for WW and WZ Resonances Decaying to Electron, Missing E_T , and Two Jets in $p\bar{p}$ Collisions at $\sqrt{s} = 1.96 \text{ TeV}$,” *Phys. Rev. Lett.* **104**, 241801 (2010), arXiv:1004.4946 [hep-ex].
- [46] Shaaban Khalil, “TeV-scale gauged B-L symmetry with inverse seesaw mechanism,” *Phys. Rev.* **D82**, 077702 (2010), arXiv:1004.0013 [hep-ph].
- [47] F. Staub, “SARAH,” (2008), arXiv:0806.0538 [hep-ph].
- [48] Florian Staub, “SARAH 4 : A tool for (not only SUSY) model builders,” *Comput. Phys. Commun.* **185**, 1773–1790 (2014), arXiv:1309.7223 [hep-ph].
- [49] Werner Porod, “SPheno, a program for calculating supersymmetric spectra, SUSY particle decays and SUSY particle production at e^+e^- colliders,” *Comput. Phys. Commun.* **153**, 275–315 (2003), arXiv:hep-ph/0301101 [hep-ph].
- [50] W. Porod and F. Staub, “SPheno 3.1: Extensions including flavour, CP-phases and models beyond the MSSM,” *Comput. Phys. Commun.* **183**, 2458–2469 (2012), arXiv:1104.1573 [hep-ph].
- [51] Benjamin W. Lee, C. Quigg, and H. B. Thacker, “Weak Interactions at Very High-Energies: The Role of the Higgs Boson Mass,” *Phys. Rev.* **D16**, 1519 (1977).
- [52] Rita Coimbra, Marco O. P. Sampaio, and Rui Santos, “ScannerS: Constraining the phase diagram of a complex scalar singlet at the LHC,” *Eur. Phys. J.* **C73**, 2428 (2013), arXiv:1301.2599 [hep-ph].
- [53] D. C. Kennedy and B. W. Lynn, “Electroweak Radiative Corrections with an Effective Lagrangian: Four Fermion Processes,” *Nucl. Phys.* **B322**, 1–54 (1989).
- [54] Michael E. Peskin and Tatsu Takeuchi, “A New constraint on a strongly interacting Higgs sector,” *Phys. Rev. Lett.* **65**, 964–967 (1990).
- [55] I. Maksymyk, C. P. Burgess, and David London, “Beyond S, T and U,” *Phys. Rev.* **D50**, 529–535 (1994), arXiv:hep-ph/9306267 [hep-ph].
- [56] Philip Bechtle, Oliver Brein, Sven Heinemeyer, Oscar Stl, Tim Stefaniak, Georg Weiglein, and Karina E. Williams, “HiggsBounds – 4: Improved Tests of Extended Higgs Sectors against Exclusion Bounds from LEP, the Tevatron and the LHC,” *Eur. Phys. J.* **C74**, 2693 (2014), arXiv:1311.0055 [hep-ph].
- [57] Philip Bechtle, Sven Heinemeyer, Oscar Stl, Tim Stefaniak, and Georg Weiglein, “HiggsSignals: Confronting arbitrary Higgs sectors with measurements at the Tevatron and the LHC,” *Eur. Phys. J.* **C74**, 2711 (2014), arXiv:1305.1933 [hep-ph].
- [58] Peter Z. Skands *et al.*, “SUSY Les Houches accord: Interfacing SUSY spectrum calculators, decay packages, and event generators,” *JHEP* **07**, 036 (2004), arXiv:hep-ph/0311123 [hep-ph].
- [59] J. Alwall, R. Frederix, S. Frixione, V. Hirschi, F. Maltoni, O. Mattelaer, H. S. Shao, T. Stelzer, P. Torrielli, and M. Zaro, “The automated computation of tree-level and next-to-leading order differential cross sections, and their matching to parton shower simulations,” *JHEP* **07**, 079 (2014), arXiv:1405.0301 [hep-ph].
- [60] Ayres Freitas, Joseph Lykken, Stefan Kell, and Susanne Westhoff, “Testing the Muon $g-2$ Anomaly at the LHC,” *JHEP* **05**, 145 (2014), [Erratum: *JHEP*09,155(2014)], arXiv:1402.7065 [hep-ph].
- [61] Stephen M. Barr and A. Zee, “Electric Dipole Moment of the Electron and of the Neutron,” *Phys. Rev. Lett.* **65**, 21–24 (1990), [Erratum: *Phys. Rev. Lett.*65,2920(1990)].

- [62] Victor Ilisie, “New Barr-Zee contributions to $(g - 2)_\mu$ in two-Higgs-doublet models,” JHEP **04**, 077 (2015), arXiv:1502.04199 [hep-ph].
- [63] Tai-Fu Feng and Xiu-Yi Yang, “Renormalization and two loop electroweak corrections to lepton anomalous dipole moments in the standard model and beyond (I): Heavy fermion contributions,” Nucl. Phys. **B814**, 101–141 (2009), arXiv:0901.1686 [hep-ph].